Properties of mouse connexin 30.2 and human connexin 31.9 hemichannels: Implications for atrioventricular conduction in the heart

Feliksas F. Bukauskas*†, Maria M. Kreuzberg‡, Mindaugas Rackauskas*, Angele Bukauskiene*, Michael V. L. Bennett*†, Vytas K. Verselis*, and Klaus Willecke‡

*Department of Neuroscience, Albert Einstein College of Medicine, 1300 Morris Park Avenue, Bronx, NY 10461; and ‡Institut für Genetik, Abteilung Molekulargenetik, Universität Bonn, Römerstrasse 164, 53117 Bonn, Germany

Contributed by Michael V. L. Bennett, May 2, 2006

Four connexins (Cxs), mouse (m)Cx30.2, Cx40, Cx43, and Cx45, determine cell–cell electrical signaling in mouse heart, and Cx43 and Cx45 are known to form unapposed hemichannels. Here we show that mCx30.2, which is most abundantly expressed in sinoatrial and atrioventricular nodal regions of the heart, and its putative human ortholog, human (h)Cx31.9, also form functional hemichannels, which, like mCx30.2 cell–cell channels, are permeable to cationic dyes up to ≈400 Da in size. DAPI uptake by HeLa cells expressing mCx30.2 was >10-fold faster than that by HeLa parental cells. In Ca^{2+}-free medium, uptake of DAPI by HeLaCx30.2-EGFP cells was increased ≈2-fold, but uptake by parental cells was not affected. Conversely, acidification by application of CO_2 reduced DAPI uptake by HeLaCx30.2-EGFP cells but had little effect on uptake by parental cells. Cells expressing mCx30.2 exhibited higher rates of DAPI uptake than did cells expressing any of the other cardiac Cxs. Cardiomyocytes of 2-day-old rats transfected with hCx31.9-EGFP took up DAPI and ethidium bromide 5–10 times faster than wild-type cardiomyocytes. Mefloquine, a close derivative of quinine and quinidine that exhibits antimalarial and antiarrhythmic properties, reduced conductance of cell–cell junctions and dye uptake through mCx30.2 hemichannels with approximately the same affinity (IC_{50} = ≈10 μM) and increased dependence of junctional conductance on transjunctional voltage. Unitary conductance of mCx30.2 hemichannels was ≈20 pS, about twice the cell–cell channel conductance. Hemichannels formed of mCx30.2 and hCx31.9 may slow propagation of excitation in the sinoatrial and atrioventricular nodes by shortening the space constant and depolarizing the excitable membrane.

gap junction | Wenckebach period

Gap junctions (GJs) are aggregates of cell–cell channels composed of connexins (Cxs) and mediate direct intercellular diffusion of cytoplasmic ions and small metabolites and signaling molecules. Twenty Cx genes have been identified in the mouse genome (1). Depending on the expression pattern, Cxs can form homomeric or heteromeric hemichannels and homotypic, heterotypic, or heteromeric cell–cell channels with highly divergent conductance, permeability, and gating properties (2). Until recently, Cx40, Cx43, and Cx45 were identified as the major Cxs expressed in the heart (1, 3). Cx43 is predominantly expressed in the atrial and ventricular working cardiomyocytes. Cx40 is highly expressed in the atrium and His bundle and its branches and, to a lesser extent, in the atrioventricular (AV) node. Cx45 is highly expressed in the sinoatrial (SA) and AV nodes and, to a lesser extent, in the His bundle and its branches (4–6). Recently, we reported that mouse Cx30.2 is expressed in the cardiac conduction system and at particularly high levels in the SA and AV nodes (7). We demonstrated that junctional conductance (g_j) of mCx30.2 GJs is weakly sensitive to transjunctional voltage (V_j), and that their single channel conductance (γ) is low, ≈9 pS, the smallest among the Cx family. GJ channels formed of hCx31.9, which is the putative human orthologue of mCx30.2, exhibit similar properties (8, 9).

Cx43 (10) and Cx45 (11) have been shown to form functional hemichannels. One report suggested that Cx40 hemichannels are not functional (12). Over the last several years, it has become evident that permeability of Cx-based hemichannels to metabolites can be important to cell function under normal and pathological conditions (13). Recent reports show that another class of membrane proteins, pannexins, that form cell–cell channels also form hemichannels that may be involved in paracrine signaling and mechanosensitivity (14, 15).

Here we report that mCx30.2 as well as human (h)Cx31.9, form functional hemichannels under normal perfusion conditions. By combining time-lapse imaging and whole-cell voltage-clamp methods, we demonstrate that cells expressing mCx30.2 and hCx31.9 exhibit much faster uptake of the dyes tested than cells expressing Cx43, Cx45, or Cx40, and that the rates of uptake are increased at low $[Ca^{2+}]_o$ and decreased by hemichannel blockers. We show that mCx30.2 hemichannels, like the corresponding cell–cell channels, are permeable to positively charged dyes with molecular mass less than ≈400 Da and exhibit weak sensitivity to voltage. Unitary conductance of the fully open mCx30.2 hemichannels is ≈20 pS, which is approximately double that of the cell–cell channels.

Results

Dye Uptake by Cx30.2 Transfectants. Experiments were performed on HeLa cells expressing mCx30.2. Dyes examined include (M_r of the fluorescent ion, valence): ethidium bromide (EtdBr; 314, +1); DAPI (279, +2), propidium iodide (PrI; 415, +2), and True Blue chloride (346, +2). Fig. 1 shows an example of dye uptake measurements in cocultures of HeLaCx30.2 and HeLa parental cells using time-lapse imaging. Cells were exposed for 2 h to DAPI (1 μM) and PrI (1 μM), after which the medium was changed to one containing only EtdBr (1 μM). Fig. 1*A* shows merged mCx30.2-EGFP (green) and phase-contrast (gray) images before dye application. The green fluorescence readily distinguishes HeLaCx30.2-EGFP cells from parental cells; dashed lines indicate the borders between the two types of cells. Fig. 1 *B* and *C* were recorded at 120 min from the start of time-lapse imaging, and EGFP fluorescence is merged with fluorescence of DAPI (in blue; Fig. 1*B*) and PrI (in red, but there was very little uptake; Fig. 1*C*). Fig. 1*D* was recorded at 260 min and is a merge of EGFP and EtdBr (in red). The kinetics of dye

Conflict of interest statement: No conflicts declared.

Abbreviations: GJ, gap junction; Cx, connexin; AV, atrioventricular; SA, sinoatrial; mCx, mouse Cx; hCx, human Cx; EtdBr, ethidium bromide; PrI, propidium iodide; ROI, region of interest.

†To whom correspondence may be addressed. E-mail: fbukausk@aecom.yu.edu or mbennett@aecom.yu.edu.

© 2006 by The National Academy of Sciences of the USA

www.pnas.org/cgi/doi/10.1073/pnas.0603372103

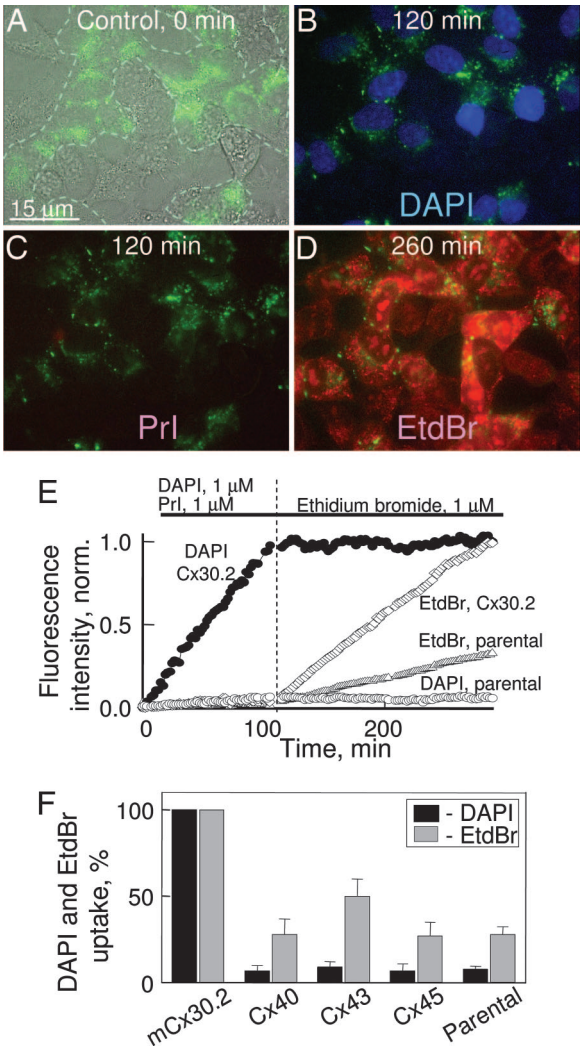

Fig. 1. Dye uptake in coculture of HeLaCx30.2 and HeLa parental cells. (*A–D*) Images at different time points of a time-lapse recording; each image has two signals superimposed. (*A*) Merged mCx30.2-EGFP (green) and phase-contrast (gray) images; dashed lines show borders between the two types of cells. (*B* and *C*) Images recorded at 120 min of time-lapse imaging show merged images of EGFP (green) with DAPI (blue, 1 μM) in *B* and with PrI (red, 1 μM, negligible staining) in *C*. (*D*) Merge of EGFP and EtdBr images recorded at 260 min of time-lapse imaging. (*E*) The kinetics of DAPI and EtdBr uptake by parental cells and cells expressing mCx30.2-EGFP; each plot is an average of fluorescence intensity from several ROI positioned on different cells (normalized for each dye to intensity measured at 300 min in mCx30.2-EGFP cells). (*F*) Histogram showing DAPI (black bars) and EtdBr (gray bars) uptake by HeLa parental cells and HeLa cells expressing different cardiac Cxs, plotted for each dye as percent uptake by HeLaCx30.2 cells.

uptake is shown in Fig. 1*E*. Each plot is an average of the fluorescence intensity measurements obtained from at least five different cells. DAPI fluorescence (filled circles) increased linearly up to 120 min when the solution was changed, and uptake was ≈18-fold greater in cells expressing mCx30.2 than in parental cells (Fig. 1*E*, open squares and triangles). PrI fluorescence was very low and near the threshold of detection in both types of cells. On changing the medium at 120 min to one containing EtdBr, DAPI fluorescence remained constant in mCx30.2 and parental cells. EtdBr fluorescence increased almost linearly for another 240 min, about three times as rapidly in mCx30.2 cells as in parental cells. On average, the rate of DAPI and EtdBr uptake by HeLaCx30.2 cells was 11.8 ± 1.3- (n = 40) and 3.6 ± 0.5- (n = 33) fold, respectively, higher than by HeLa parental cells. Movies 1 and 2, which are published as supporting information on the PNAS web site, show uptake of dyes from the experiment shown in Fig. 1.

Uptake of True Blue chloride, which has a molecular mass of 346 Da, between that of DAPI and PrI, and the same valence (z = +2), was on average 2.2 ± 0.5-fold (n = 5) faster in cells expressing mCx30.2 than in parental cells. HeLaCx30.2 cells showed little PrI uptake even after a 24-h period of imaging (≈1–3% relative to EtdBr or DAPI uptake; this difference cannot be due to lower fluorescence efficiency of PrI, because extinction coefficients and quantum yields of EtdBr and PrI are similar when bound to cell constituents (Molecular Probes). Therefore, our data suggest that compounds of M_r > ≈400 Da and z = +2 do not permeate mCx30.2 hemichannels.

We also evaluated dye uptake by HeLa cells expressing three other cardiac Cxs, Cx40, Cx43, and Cx45; dye concentrations were ≈1 μM or less if specified. The average rate of uptake of DAPI (black bars) and EtdBr (gray bars) by HeLa parental cells and cells expressing one of the four cardiac Cxs are summarized in Fig. 1*F* (plotted as percentage of the rate of uptake of each dye by Cx30.2 cells; expression levels of the Cxs were similar, as determined from whole-cell fluorescence of the EGFP tag). It was reported previously that Cx43 (10) and Cx45 (11) form functional hemichannels. DAPI uptake was not significantly different in HeLa cells expressing Cx40-EGFP, Cx43-EGFP, or Cx45-EGFP than in parental cells (number of experiments, n = 8, P > 0.05). Thus, the ratio of DAPI uptake mediated by mCx30.2 hemichannels to that mediated by hemichannels formed by the other cardiac Cxs may be much greater than the ≈10-fold difference observed in total uptake. EtdBr uptake was ≈2-fold higher in HeLaCx43-EGFP than in parental cells in agreement with reported data (10) but was not significantly different in HeLa cells expressing Cx40 (n = 9; P > 0.05) or Cx45 (n = 5, P > 0.05) and in parental cells. As for DAPI, the ratio of EtdBr uptake mediated by mCx30.2 hemichannels to that mediated by those formed by Cx40 or Cx45 may be much larger than the ≈3-fold ratio of total uptake. Electrophysiological studies in *Xenopus* oocytes suggest that Cx40 hemichannels are not functional (12). Cx45 hemichannel activity reported previously (10) was observed only in physiological salt solution with no added Ca^{2+}, which accounts for the lack of uptake in our experiments in normal (2 mM) Ca^{2+} (12). Thus, despite the small unitary conductance of mCx30.2 hemichannels (see below), cells expressing mCx30.2-EGFP permit greater dye uptake in normal Ca^{2+} than cells expressing other cardiac Cxs, even at similar expression levels assessed by Cx-EGFP fluorescence. Uptake through hemichannels is determined by surface expression, open probability, and single channel permeability. As argued below, we think that the greater uptake by cells expressing mCx30.2 is because of greater open probability rather than increased surface expression and occurs despite lower single channel permeability.

Lowering of $[Ca^{2+}]_o$ has been shown to increase opening of hemichannels formed of Cx43, Cx45, Cx46, Cx50, and Cx56 (10, 11, 16, 17). To examine whether lowering $[Ca^{2+}]_o$ also increases dye uptake consistent with increased opening of mCx30.2 hemichannels, we exposed HeLa parental cells as well as HeLa cells expressing mCx30.2-EGFP or EGFP alone to a nominally Ca-free solution after ≈1 h in Krebs–Ringer solution containing 2 mM Ca^{2+}; both solutions contained DAPI (1 μM) and either EtdBr (0.1 μM) or PrI (1 μM). Application of Ca-free solution increased the rate of DAPI uptake to about twice the control value in cells expressing mCx30.2 (Fig. 2 *A* and *D*) but had little or no effect on uptake by parental cells (Fig. 2*A*). The effect of Ca-free conditions on mCx30.2 cells was relatively fast, reaching a new steady state in less than the time between images, ≈1 min. Exposure to Ca-free conditions increased EtdBr uptake by

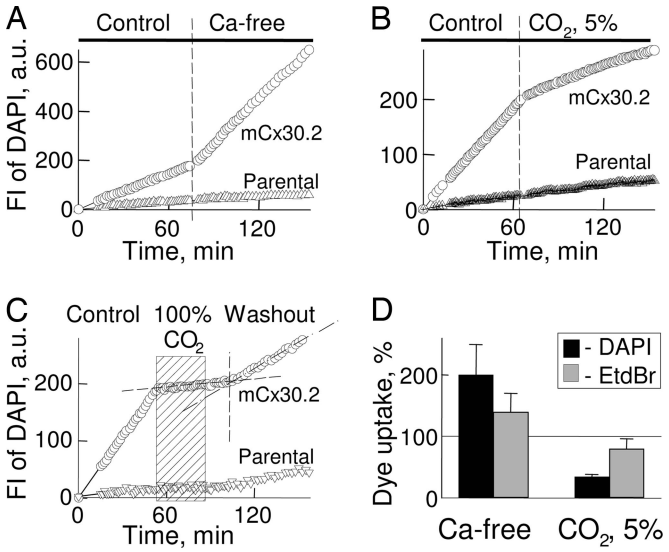

Fig. 2. DAPI and EtdBr uptake is increased by lowering $[Ca^{2+}]_o$ and decreased by lowering pH. (*A* and *B*) Selected examples that illustrate changes in rate of DAPI uptake (1 μM) by HeLa cells expressing mCx30.2-EGFP (circles) and parental cells (triangles) after exposure to Ca-free conditions (*A*) and 5% CO_2 (*B*); under control conditions, the cells were exposed to Krebs–Ringer solution equilibrated with air. (*C*) Medium equilibrated with 100% CO_2 caused an almost complete block of DAPI uptake by HeLaCx30.2 cells (see region defined by the cross-hatched rectangle). (*D*) Averaged data ($n = 6$) of effects (normalized as percent of uptake in control solution) of Ca-free conditions and of 5% CO_2 on rate of uptake of DAPI (black bars) and EtdBr (gray bars) by HeLaCx30.2-EGFP cells.

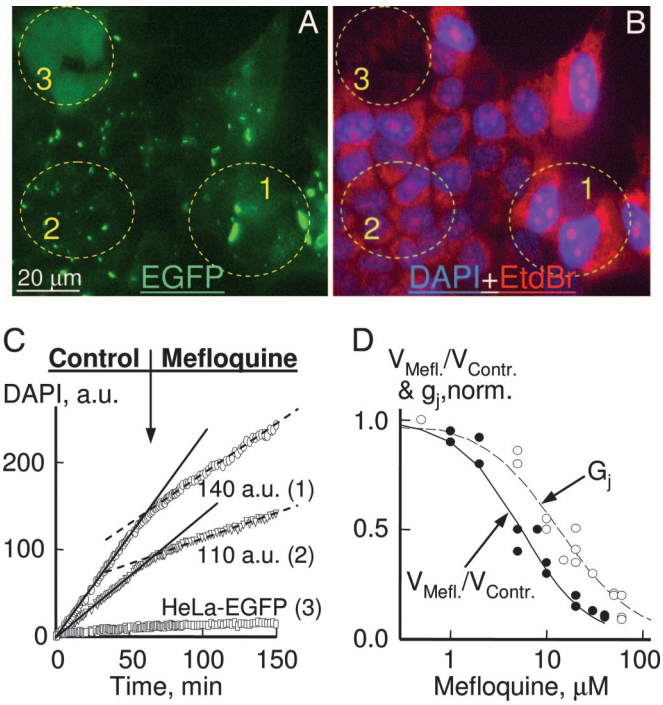

Fig. 3. Mefloquine blocks mCx30.2-EGFP GJ channels and hemichannels. (*A*) Image shows coculture of HeLaCx30.2-EGFP cells (punctate green, regions 1 and 2) and HeLa EGFP cells (diffuse green, region 3). (*B*) Merged images of nuclei staining by DAPI (blue) and cytoplasm and nucleoli stained by EtdBr (red) in regions 1 and 2 and faint EtdBr staining of HeLa EGFP cells in region 3 after ≈2 h exposure to dyes. (*C*) Illustration of DAPI uptake over time by measuring fluorescence from regions shown in *A* and *B*; ROI 1 and 2 are positioned on HeLaCx30.2-EGFP cells exhibiting more and less intense EGFP fluorescence, respectively. Rate of uptake was greater for region 1, which had a mean fluorescence intensity of 140 arbitrary units (a.u.), than for region 2, which had a fluorescence intensity of 110 a.u. Uptake was just detectable in region 3. (*D*) Normalized effect-concentration plots that demonstrate decrease in the rate of DAPI uptake (filled circles) and in g_j (open circles) as a function of the concentration of mefloquine. Curves are fits of a Hill equation to the experimental data to estimate concentrations for half-maximal inhibition (IC_{50}) and sensitivity (n) coefficients.

≈40% compared to control conditions (Fig. 2*D*, $n = 6$). PrI uptake was minimal or undetectable and showed no difference between HeLa parental and HeLaCx30.2 cells with or without Ca^{2+} added to the bath (data not shown, $n = 4$).

To verify mediation of dye uptake by hemichannels, we used several treatments that block hemichannels in other systems, including low pH (18), La^{3+} (reviewed in ref. 19), and mefloquine (17). Mefloquine is a close derivative of quinine and quinidine, which are used as antimalarial and antiarrhythmic drugs, and we wanted to determine whether its effect on mCx30.2 hemichannels and cell–cell channels could contribute to the effects observed in clinical studies.

Acidification of cells by exposure to Krebs–Ringer solution, equilibrated with air containing 5% CO_2 instead of normal room air (≈0.04% CO_2), reduced pH of the solution from 7.4 to ≈6.25 and reduced dye uptake by mCx30.2 cells but not by parental cells (Fig. 2*B*). On average, the CO_2 solution reduced the rate of DAPI uptake by ≈70% and of EtdBr uptake by ≈20% (Fig. 2*D*, right bars, $n = 6$). Exposure to 100% CO_2 almost completely blocked dye uptake in cells expressing mCx30.2-EGFP and caused a slight reduction in the basal uptake observed in parental cells as well (Fig. 2*C*). We used the pH dependence of EGFP to evaluate pH changes induced by these treatments [see extended version of Fig. 2 (Fig. 7, which is published as supporting information on the PNAS web site); pH values indicated in *Inset* (*Right*) are from a calibration plot obtained by measuring the fluorescence of isolated EGFP protein at different pH values]. Exposure to 5% CO_2 decreased EGFP fluorescence ≈20%, corresponding to an intracellular pH (pH_i) of ≈6.4. Exposure to 100% CO_2 decreased EGFP fluorescence to a level corresponding to pH_i 5.5. Recovery of DAPI uptake during washout appeared to lag pH_i recovery (see vertical dashed line, Fig. 7) and was incomplete. Because extracellular pH (pH_o) recovery presumably occurred with seconds, dye uptake appears to be sensitive to pH_i, and not pH_o, in agreement with studies of Cx46 hemichannels, which indicated a cytoplasmic site for H^+ action (18). Block and recovery of EtdBr uptake with 100% CO_2 treatment were similar to that shown for DAPI (data not shown).

Shortly after exposure to 100% CO_2, the movement of the intracellular organelles ceased, and with longer exposures, cell viability was compromised. Organelle movement partially recovered during washout, when intracellular pH reached ≈6.4.

Mefloquine at low concentrations (≈1 μM) blocks both GJ channels and hemichannels composed of Cx36 and Cx50 (17, 20). Other Cxs are sensitive to mefloquine to varying degrees (20), and we used mefloquine concentrations ranging from 0.5 to 40 μM. Fig. 3*B* is a merged image showing DAPI (blue) and EtdBr (red) uptake in coculture of HeLaCx30.2-EGFP cells [EGFP fluorescence that is punctate, areas 1 and 2 (Fig. 3*A*)] and HeLa-EGFP cells (EGFP fluorescence that is diffuse, area 3 in Fig. 3*A*) after exposure to dyes for 1 h in control solution and then for 1.5 h with mefloquine added. Dye uptake over time was evaluated by examining fluorescence from regions of interest (ROI) positioned on HeLaCx30.2-EGFP cells (ROI 1 and 2) and HeLa-EGFP cells (ROI 3). It was our impression that uptake of both dyes was faster in cells with higher expression of mCx30.2-EGFP. In Fig. 2*A*, 140 and 110 are mean fluorescence intensities of EGFP measured in arbitrary units from ROI 1 and 2, respectively. Obviously, this macroscopic measurement will not

necessarily reflect surface expression, a more likely valid correlate of rate of uptake. Mefloquine (5 μM) decreased the rate of dye uptake by ≈50% (Fig. 3*C*). The ratio of steady-state rate of uptake during application of mefloquine to that under control conditions, V_{Mefl}/V_{Contr}, decreased with mefloquine in a concentration-dependent manner (Fig. 3*D*, filled circles). A Hill equation was fit to the data (see solid line) to estimate concentration of half-maximal inhibition (IC_{50}) and coefficient of sensitivity (n); IC_{50} = 5.5 μM and n = 1.3.

In addition, La^{3+} (50–100 μM for 30–40 min; n = 7) rapidly (less than a few minutes) reduced DAPI and EtdBr uptake by 70–90%, but recovery of uptake during washout was absent or very slow, and after ≈4–5 h of time-lapse imaging, both parental and mCx30.2 cells exhibited blebbing of the plasma membrane and disintegration of cell structure. Similar structural damage was not observed during time-lapse imaging for >12 h when we examined the effects of mefloquine, 5% CO_2, or Ca-free conditions.

In summary, enhanced dye uptake in mCx30.2 transfectants compared to parental cells in control and under Ca-free conditions and blocking of dye uptake by acidification, mefloquine, and La^{3+} provide evidence that mCx30.2 indeed forms functional hemichannels. We found no difference between parental cells and cells expressing only EGFP in uptake of any dye examined; thus, the transfection vector is unlikely to account for differences in dye uptake.

***g*$_j$ and Voltage Sensitivity, Effect of Mefloquine.** To examine whether mefloquine also affects mCx30.2-based GJ channels, we measured g_j in mCx30.2-EGFP cell pairs by dual whole-cell voltage clamp. Fig. 3*C* (open circles, fitted with a dashed line) shows a plot of the dependence of G_j (g_j normalized to its value at V_j = 0) on mefloquine concentration (Hill parameters: IC_{50} = 13 μM and n = 1.2). At concentrations of 5–15 μM, uncoupling was not complete, and recovery was relatively slow, which allowed us to study the effect of mefloquine on V_j gating. Mefloquine transformed mCx30.2 GJ channels from being relatively insensitive to V_j (7) to being moderately sensitive. In Fig. 4*A*, g_j (bottom trace; $g_j = I_j/V_j$) was monitored by applying repeated voltage ramps of small amplitude (from −20 to +20 mV at once per 2 s; ramp duration of 1.7 s). Positive V_j steps were applied to examine V_j sensitivity. Before addition of mefloquine, g_j increased during a 100-mV positive V_j step from ≈11 to 17.5 nS and slowly recovered upon termination of the V_j step. This result is consistent with the g_j increase at moderate V_js shown earlier (7) and suggests that a fraction of the cell–cell channels are closed under normal conditions. During application of 15 μM mefloquine, g_j decreased at the holding potential (to ≈3 nS) until washout was started after ≈250 s (≈10 s before the end of the break in the recording displayed in Fig. 4). During this period, positive steps transiently decreased g_j further and with increasing efficacy; g_j largely recovered between steps. The time course of the decrease and recovery in response to a V_j step was slow (although faster than the action of mefloquine) and without a fast component, as seen from the exponential fit to the g_j data after the V_j step (gray line indicated by the arrow in Fig. 4*A Inset*). Although most GJ channels and hemichannels have been shown to contain two gating mechanisms (21, 22), the slow kinetics of V_j dependence may mean that operation of the slow gate predominates over the fast one under these conditions.

Fig. 4*B* shows G_j–V_j dependence measured by applying long V_j ramps (150 s; from 0 to +110 mV and from 0 to −110 mV with a 150-s interval between them) under control conditions and in the presence of mefloquine (10 μM). Under control conditions, g_j increased at moderate V_js and decreased at higher V_js. Only decreases in g_j were observed in the presence of mefloquine. The white solid line is a Boltzmann relation fit to the data (see *Supporting Text*, which is published as supporting information on the PNAS web site). Both plots, with and without mefloquine, show some gating asymmetry with higher gating sensitivity for positive V_js; thus, there may be some degree of dependence on transmembrane voltage. We expect that the action of mefloquine on g_j was not constant during application of the V_j ramp; however, application of either steps or ramps showed increase in V_j-gating sensitivity in the presence of mefloquine. Conductances at which we measured V_j gating in the presence of mefloquine were in the range of several nanosiemens, i.e., greater than conductances typically measured between HeLa parental cells, indicating that the observed effects were not because of endogenous Cx45, which is expressed at low levels in HeLa cells. Moreover, Cx45 junctions are much more voltage-sensitive than mCx30.2 junctions even in the presence of mefloquine

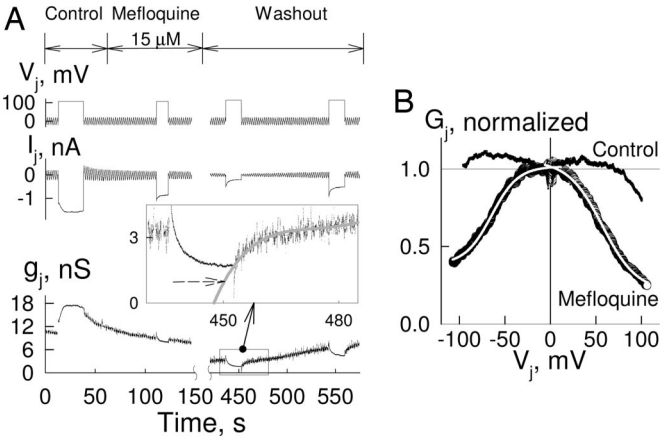

Fig. 4. Mefloquine reduces g_j and increases V_j-gating sensitivity of mCx30.2 junctions. (*A*) I_j and g_j responses to voltage steps of 100 mV and repeated voltage ramps of small amplitude (see V_j trace) show that mefloquine reduces g_j. In control saline, I_j tended to increase in response to a 100-mV voltage step, whereas in the presence of mefloquine, I_j decreased during a V_j step of the same magnitude (see *Results*). The break in the record was ≈260 s long; washout of mefloquine was begun at ≈400 s. (*B*) G_j-V_j plots recorded in response to long V_j ramps (V_j changed during 180 s from 0 to −110 mV and from 0 to +110 mV) under control conditions (data points in black) and in the presence of mefloquine (15 μM; data points in circles). Fit of the data measured in mefloquine to the Boltzmann equation is shown by the white solid line; fitting parameters are as follows: b = 0.06 and 0.05, V_o = −65 and 57 mV and g_{min} = 0.38 and 0.21, respectively, for negative and positive V_js.

Dye Uptake by HeLa Cells and Cardiomyocytes Expressing hCx31.9-EGFP. Cell–cell channels formed by the putative human ortholog of mCx30.2, hCx31.9, also exhibit low sensitivity to V_j and a small unitary conductance (8, 9). In cocultures of HeLa parental cells and cells expressing hCx31.9-EGFP, the rate of DAPI and EtdBr uptake by HeLaCx31.9-EGFP cells was 11 ± 2-fold (n = 9) and 3.7 ± 0.8-fold (n = 10), respectively, higher than by HeLa parental cells. Thus, hCx31.9 hemichannels show properties similar to those of mCx30.2 hemichannels (see Movie 3, which is published as supporting information on the PNAS web site). Ca-free medium increased and mefloquine decreased uptake of DAPI and EtdBr by hCx31.9 cells, as in cells expressing mCx30.2 (data not shown).

To examine the function of hCx31.9 hemichannels in cardiomyocytes, we transfected 2-day-old cultures of cardiac myocytes from newborn rats with hCx31.9-EGFP. The cardiomyocytes were exposed to the transfection vector (pMJ) containing hCx31.9-EGFP DNA and Lipofectamine-2000. Transfected and nontransfected cells demonstrated spontaneous contractility with no visually detectable differences in their structure. When two cardiomyocytes expressing hCx31.9-EGFP were in contact, they often formed junctional plaques in their appositional region (arrow in Fig. 5*A*). Five experiments from different transfections

PHYSIOLOGY

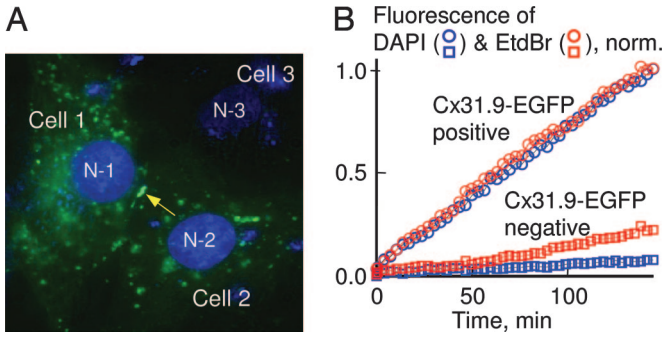

Fig. 5. hCx31.9 forms functional hemichannels in cardiomyocytes. (*A*) Merge of EGFP (in green) and DAPI (in blue) fluorescence images of a monolayer of a 2-day-old culture of cardiac myocytes isolated from newborn rats and transfected with hCx31.9-EGFP. Cells 1 and 2 are contacting cardiac myocytes expressing hCx31.9-EGFP, form a junctional plaque (arrow), and exhibit higher uptake of DAPI than a nontransfected cell, Cell 3; N1–N3 are nuclei of the cells. DAPI (2 μM) was applied to these cells for 4 h. (*B* and *C*) Uptake of DAPI (*C*) and EtdBr (*D*) by cardiomyocytes expressing hCx31.9-EGFP (blue and red open circles, respectively) was faster than that by wild-type cardiomyocytes (blue and red open squares). For each dye, fluorescence is normalized to the final value in the transfected cells.

were performed, and in all of them we observed that cardiomyocytes expressing hCx31.9-EGFP demonstrated faster uptake of both DAPI and EtdBr than wild-type cardiomyocytes [Fig. 5*A*; merge of EGFP (green) and DAPI (blue) images]. Fig. 5*B* shows the time course of the uptake of DAPI (blue symbols) and EtdBr (red symbols) normalized to the final value in the transfected cells. The ratio of rates of dye uptake by transfected (circles) and nontransfected (squares) cardiomyocytes was greater for DAPI than for EtdBr.

Electrophysiological Studies of Hemichannel Function. To examine mCx30.2 hemichannel function electrophysiologically, we performed whole-cell recording from single HeLa cells expressing

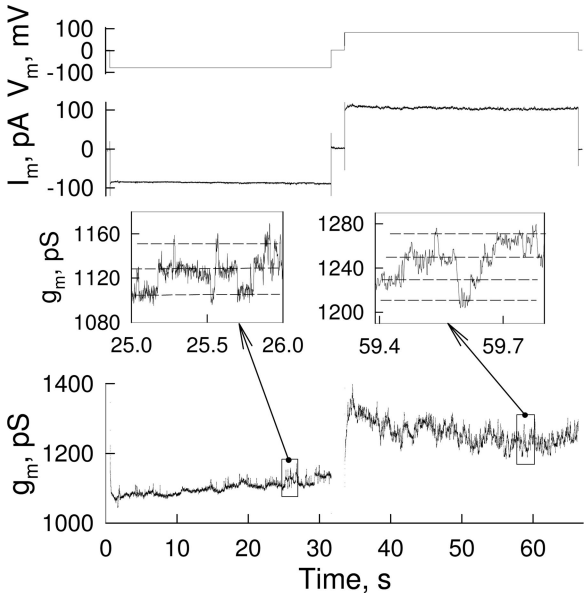

Fig. 6. Unitary gating events measured in a HeLa cell expressing mCx30.2-EGFP. Whole cell current (I_m, middle trace) and conductance (g_m, lower trace and *Insets*) are shown for voltage steps of ±80 mV. Unitary gating events of ≈20 pS in amplitude can be seen in two *Insets* as transitions between different levels of g_m (indicated by dashed horizontal lines).

mCx30.2-EGFP under normal conditions. Fig. 6 shows whole-cell conductance (g_m trace calculated as the ratio of whole-cell current, I_m, to transmembrane voltage, V_m) during V_m steps (Fig. 6 *Top*). I_m recordings in this and other experiments with HeLa mCx30.2 cells ($n = 24$) revealed small unitary gating events of ≈20 pS in magnitude (see dashed lines in the two *Insets*), which were not observed in parental cells. Typically, the frequency of gating events was not greatly affected during long V_m steps, consistent with the weak voltage dependence of mCx30.2 GJ channels. In both HeLa parental and mCx30.2 cells, we occasionally observed unitary events of 35–80 pS, mainly at positive V_ms. These events can be attributed to endogenous Cx45 hemichannels (11) or possibly other types of ion channels.

Discussion

From numerous reports during the last several years, it has become evident that the permeability of Cx-based hemichannels to metabolites is important to cell function under normal and pathological conditions in different organs and tissues (13, 23). Biophysical properties of Cx43 and Cx45 hemichannels have already been examined (10, 11). Both electrophysiological studies in *Xenopus* oocytes expressing Cx40 (12) and failure of Cx40 expression by HeLa cells to increase dye uptake indicate that Cx40 hemichannels are closed under normal perfusion conditions. Similarly, Cx45 hemichannels are probably closed at normal Ca^{2+} levels. Here we demonstrate the function of mCx30.2 hemichannels. Thus, in normal conditions hemichannels formed by at least two cardiac Cxs, mCx30.2 and Cx43, can contribute to ionic and metabolic exchange across the plasma membrane or in paracrine cell–cell signaling by small molecules.

We find that mCx30.2 and hCx31.9 hemichannels can be open under normal (control) conditions and allow passage of dyes up to ≈400 Da in molecular mass. The unitary conductance (γ) of mCx30.2 hemichannels is ≈20 pS, i.e., approximately that predicted from γ of the cell–cell channel assuming a simple series arrangement of hemichannels. Our cell–cell dye transfer studies show that permeability to Alexa Fluor^{350} of mCx30.2 GJ channels is significantly lower (>100-fold) than permeability of Cx43, Cx40, or Cx45 GJ channels (M.R. and F.F.B., unpublished work). Presumably, the same is true for mCx30.2 hemichannels. If so, the higher rate of dye uptake by cells expressing mCx30.2 or hCx31.9 is not because of higher permeability of single hemichannels but because of greater open probability at the resting potential. We recognize that hemichannels in the membrane may not all be in the same state, and we do not distinguish between a smaller fraction of hemichannels with a larger open probability and a larger fraction of hemichannels with a smaller open probability. Surface expression will also be a factor, but overall fluorescence measurements suggest that the difference in surface expression is likely too small to account for the great difference in DAPI uptake.

Our studies show that, under normal conditions, the ratio of rates of dye uptake by HeLaCx30.2 cells relative to uptake by HeLa parental cells is considerably greater for DAPI than for EtdBr. Presumably EtdBr uptake by pathways other than hemichannels is higher than DAPI uptake because of their difference in valence (+1 vs. +2). The more pronounced effects of acidification, mefloquine, and Ca-free conditions on DAPI uptake compared with EtdBr uptake are consistent with a larger fraction of DAPI uptake being mediated by hemichannels.

We show that uptake of DAPI and EtdBr by mCx30.2 cells is (*i*) markedly faster than that by cells expressing other cardiac Cxs, (*ii*) increased under low $[Ca^{2+}]_o$ conditions, and (*iii*) decreased in the presence of hemichannel blockers. mCx30.2 cell–cell channels exhibit a negative gating polarity, i.e., in response to a V_j, the hemichannel on the relatively negative side closes, but their V_j-gating sensitivity is significantly lower than that of cell–cell channels of Cx43 and Cx45, which also form

functional hemichannels (7). The low open probability of Cx43 and Cx45 hemichannels at the resting potential is possibly because of the negative resting potential and negative gating polarities of both fast and slow gates (21), and hemichannel open probability is much greater at inside positive potentials (10, 11). Therefore, mCx30.2 hemichannels may not be closed by voltage at typical resting potentials unlike hemichannels formed of Cxs with higher sensitivity to negative voltage. Taken together, these data may explain why cells expressing mCx30.2 hemichannels exhibit faster dye uptake than cells expressing other cardiac Cxs

Dye uptake mediated by mCx30.2-EGFP hemichannels does not appear to be affected by the EGFP tag, because we observed similar dye uptake in HeLa cells expressing wild-type mCx30.2. Expression of hCx31.9-EGFP by cultured cardiomyocytes markedly increased their permeability to dyes, suggesting that mCx30.2 and hCx31.9 hemichannels might behave similarly in the heart and in HeLa transfectants.

mCx30.2 knockout mice show enhanced AV conduction and a reduced Wenckebach period, which defines the smallest time interval between atrial impulses that will propagate through the AV node to the ventricles (24). The deletion of the mCx30.2 gene did not result in overexpression of Cx40, Cx43, or Cx45 that could explain enhanced AV conduction. We envision two mechanisms that may explain why the velocity of propagation increases. Opening the mCx30.2 hemichannels in cardiomyocytes would reduce membrane resistance, R_m, and the length constant and lead to depolarization, which could depress the action potential mechanism (25, 26). These changes could slow conduction in the SA and AV nodes, which express mCx30.2 at high levels. This explanation is consistent with the fact that ablation of mCx30.2 does not lead to prolongation of P and QRS waves, which indicates that the velocity of conduction in atria and ventricles does not change (24). In addition or alternatively, mCx30.2 can exert a dominant negative effect on the function of other cardiac Cxs. As we previously reported, homo- as well as heterotypic GJ channels containing mCx30.2 exhibit unitary conductances that are very small, typically <18 pS (7). It is possible, but not yet tested, that heteromeric hemichannels and GJ channels containing mCx30.2 can also be formed, and that they exhibit low γ or low open channel probability. Thus, we assume that in the absence of mCx30.2, combinations of Cx40, Cx43, and Cx45 can form GJ channels with higher γs, resulting in higher conduction velocity. mCx30.2 ablation should lead to a net reduction in total hemichannel conductance.

The opening of the mCx30.2 hemichannels raises the question why cells would waste energy by forming a leak across the plasma membrane through mCx30.2 hemichannels instead of expressing fewer GJ channels in the AV node to slow propagation. The solution of having a functionally balanced conductance for both cell–cell junctions and hemichannels presumably represents a compromise to fulfill functional requirements, e.g., slowing conduction and protecting ventricles from overexcitation during atrial tachycardia.

Methods

Functional Cloning, Cell Cultures, and Transfection. The coding regions of mCx30.2 and hCx31.9 were cloned into pIRESpuro2 or pIRESpuro2-EGFP vectors, which were transfected into HeLa cells as described (7). For control, we used HeLa parental cells and HeLa cells expressing EGFP alone.

Electrophysiology and Fluorescence Imaging. The dual whole-cell voltage-clamp method was used for electrophysiological studies (27). For time-lapse recording of dye uptake, we used a microincubator adapted to fit on the stage of an inverted microscope and a Hamamatsu Photonics (Hamamatsu City, Japan) digital camera operated by ULTRAVIEW (PerkinElmer) imaging software.

Expanded methods may be found in *Supporting Text*.

We thank Drs. David Spray and Silvia Suadicani (Albert Einstein College of Medicine) for providing the isolated cardiomyocytes and Dr. Miduturu Srinivas (The State University of New York College of Optometry, New York) for the mefloquine. This work was supported by National Institutes of Health Grants R01 NS036706 (to F.F.B.), GM54179 (to V.K.V.), and NS45837 (to M.V.L.B.) and German Research Association Grant Wi 270/29-1 (to K.W.).

1. Sohl, G. & Willecke, K. (2004) *Cardiovasc. Res.* **62,** 228–232.
2. Harris, A. L. (2001) *Q. Rev. Biophys.* **34,** 325–427.
3. Severs, N. J., Dupont, E., Coppen, S. R., Halliday, D., Inett, E., Baylis, D. & Rothery, S. (2004) *Biochim. Biophys. Acta* **1662,** 138–148.
4. Gros, D. B. & Jongsma, H. J. (1996) *BioEssays* **18,** 719–730.
5. Lo, C. W. (2000) *Circ. Res.* **87,** 346–348.
6. van Rijen, H. V., van Veen, T. A., van Kempen, M. J., Wilms-Schopman, F. J., Potse, M., Krueger, O., Willecke, K., Opthof, T., Jongsma, H. J. & de Bakker, J. M. (2001) *Circulation* **103,** 1591–1598.
7. Kreuzberg, M. M., Sohl, G., Kim, J., Verselis, V. K., Willecke, K. & Bukauskas, F. F. (2005) *Circ. Res.* **96,** 1169–1177.
8. Nielsen, P. A., Beahm, D. L., Giepmans, B. N., Baruch, A., Hall, J. E. & Kumar, N. M. (2002) *J. Biol. Chem.* **277,** 38272–38283.
9. White, T. W., Srinivas, M., Ripps, H., Trovato-Salinaro, A., Condorelli, D. F. & Bruzzone, R. (2002) *Am. J. Physiol. Cell Physiol.* **283,** C960–C970.
10. Contreras, J. E., Saez, J. C., Bukauskas, F. F. & Bennett, M. V. L. (2003) *Proc. Natl. Acad. Sci. USA* **100,** 11388–11393.
11. Valiunas, V. (2002) *J. Gen. Physiol.* **119,** 147–164.
12. Beahm, D. L. & Hall, J. E. (2004) *Biophys. J.* **86,** 781–796.
13. Bennett, M. V. L., Contreras, J. E., Bukauskas, F. F. & Saez, J. C. (2003) *Trends Neurosci.* **26,** 610–617.
14. Bruzzone, R., Barbe, M. T., Jakob, N. J. & Monyer, H. (2005) *J. Neurochem.* **92,** 1033–1043.
15. Bao, L., Sachs, F. & Dahl, G. (2004) *Am. J. Physiol.* **287,** C1389–C1395.
16. Ebihara, L. & Steiner, E. (1993) *J. Gen. Physiol.* **102,** 59–74.
17. Srinivas, M., Kronengold, J., Bukauskas, F. F., Bargiello, T. A. & Verselis, V. K. (2005) *Biophys. J.* **88,** 1725–1739.
18. Trexler, E. B., Bukauskas, F. F., Bennett, M. V. L., Bargiello, T. A. & Verselis, V. K. (1999) *J. Gen. Physiol* **113,** 721–742.
19. Saez, J. C., Retamal, M. A., Basilio, D., Bukauskas, F. F. & Bennett, M. V. L. (2005) *Biochim. Biophys. Acta* **1711,** 215–224.
20. Cruikshank, S. J., Hopperstad, M., Younger, M., Connors, B. W., Spray, D. C. & Srinivas, M. (2004) *Proc. Natl. Acad. Sci. USA* **101,** 12364–12369.
21. Bukauskas, F. F. & Verselis, V. K. (2004) *Biochim. Biophys. Acta* **1662,** 42–60.
22. Verselis, V. K. & Bukauskas, F. F. (2002) *Curr. Drug Targets* **3,** 483–499.
23. John, S. A., Kondo, R., Wang, S. Y., Goldhaber, J. I. & Weiss, J. N. (1999) *J. Biol. Chem.* **274,** 236–240.
24. Kreuzberg, M., Schrickel, J., Ghanem, A., Kim, J., Degen, J., Janssen-Bienhold, U., Lewalter, T., Tiemann, K. & Willecke, K. (2006) *Proc. Natl. Acad. Sci. USA* **108,** 5959–5964.
25. Meijler, F. L. & Janse, M. J. (1988) *Physiol. Rev* **68,** 608–647.
26. Kleber, A. G. & Rudy, Y. (2004) *Physiol. Rev* **84,** 431–488.
27. Bukauskas, F. F. (2001) *Methods Mol. Biol.* **154,** 379–393.